



Search for Low-energy Electron Antineutrinos in KamLAND Associated with Gravitational Wave Events

S. Abe¹, S. Asami¹, A. Gando¹, Y. Gando¹, T. Gima¹, A. Goto¹, T. Hachiya¹, K. Hata¹, S. Hayashida^{1,21}, K. Hosokawa¹, K. Ichimura¹, S. Ieki¹, H. Ikeda¹, K. Inoue^{1,2}, K. Ishidoshiro¹, Y. Kamei¹, N. Kawada¹, Y. Kishimoto^{1,2}, T. Kinoshita¹, M. Koga^{1,2}, N. Maemura¹, T. Mitsui¹, H. Miyake¹, K. Nakamura¹, K. Nakamura¹, R. Nakamura¹, H. Ozaki^{1,3}, T. Sakai¹, H. Sambonsugi¹, I. Shimizu¹, J. Shirai¹, K. Shiraishi¹, A. Suzuki¹, Y. Suzuki¹, A. Takeuchi¹, K. Tamae¹, K. Ueshima^{1,22}, Y. Wada¹, H. Watanabe¹, Y. Yoshida¹, S. Obara⁴, A. Kozlov^{2,23}, D. Chernyak^{2,24}, Y. Takemoto^{5,25}, S. Yoshida⁵, S. Umehara⁶, K. Fushimi⁷, A. K. Ichikawa⁸, K. Z. Nakamura⁸, M. Yoshida⁸, B. E. Berger^{2,9}, B. K. Fujikawa^{2,9}, J. G. Learned¹⁰, J. Maricic¹⁰, S. N. Axani¹¹, L. A. Winslow¹¹, Z. Fu¹¹, J. Ouellet¹¹, Y. Efremenko^{2,12}, H. J. Karwowski^{13,14,17}, D. M. Markoff^{13,15}, W. Tornow^{2,13,16}, A. Li¹⁴, J. A. Detwiler^{2,17}, S. Enomoto^{2,17}, M. P. Decowski^{2,18}, C. Grant¹⁹, T. O'Donnell²⁰, and S. Dell'Oro²⁰

(KamLAND Collaboration)

¹ Research Center for Neutrino Science, Tohoku University, Sendai 980-8578, Japan

² Institute for the Physics and Mathematics of the Universe, The University of Tokyo, Kashiwa 277-8568, Japan

³ Graduate Program on Physics for the Universe, Tohoku University, Sendai 980-8578, Japan

⁴ Frontier Research Institute for Interdisciplinary Sciences, Tohoku University, Sendai, 980-8578, Japan; shuhei.obara.d4@tohoku.ac.jp

⁵ Graduate School of Science, Osaka University, Toyonaka, Osaka 560-0043, Japan

⁶ Research Center for Nuclear Physics (RCNP), Osaka University, Ibaraki, Osaka 567-0047, Japan

⁷ Graduate School of Advanced Technology and Science, Tokushima University, Tokushima, 770-8506, Japan

⁸ Department of Physics, Kyoto University, Kyoto 606-8502, Japan

⁹ Nuclear Science Division, Lawrence Berkeley National Laboratory, Berkeley, CA 94720, USA

¹⁰ Department of Physics and Astronomy, University of Hawaii at Manoa, Honolulu, HI 96822, USA

¹¹ Massachusetts Institute of Technology, Cambridge, MA 02139, USA

¹² Department of Physics and Astronomy, University of Tennessee, Knoxville, TN 37996, USA

¹³ Triangle Universities Nuclear Laboratory and Physics Departments at Duke University, North Carolina Central University, and the University of North Carolina at Chapel Hill, Durham, NC 27708, USA

¹⁴ The University of North Carolina at Chapel Hill, Chapel Hill, NC 27599, USA

¹⁵ North Carolina Central University, Durham, NC 27701, USA

¹⁶ Physics Department at Duke University, Durham, NC 27705, USA

¹⁷ Center for Experimental Nuclear Physics and Astrophysics, University of Washington, Seattle, WA 98195, USA

¹⁸ Nikhef and the University of Amsterdam, Science Park, Amsterdam, The Netherlands

¹⁹ Boston University, Boston, MA 02215, USA

²⁰ Center for Neutrino Physics, Virginia Polytechnic Institute and State University, Blacksburg, VA 24061, USA

Received 2020 December 4; revised 2020 December 17; accepted 2020 December 20; published 2021 March 10

Abstract

We present the results of a search for MeV-scale electron antineutrino events in KamLAND coincident with the 60 gravitational wave events/candidates reported by the LIGO/Virgo collaboration during their second and third observing runs. We find no significant coincident signals within a ± 500 s timing window from each gravitational wave and present 90% C.L. upper limits on the electron antineutrino fluence between 10^8 and 10^{13} cm $^{-2}$ for neutrino energies in the energy range of 1.8–111 MeV.

Key words: Neutrino astronomy – Gravitational waves

1. Introduction

In 2015, gravitational waves (GWs) were first detected by the Advanced Laser Interferometer Gravitational-wave Observatory (LIGO) (Abbott et al. 2016). This event was shown to have originated from the merger of a binary black hole (BBH) system. Nearly two years earlier, the IceCube collaboration published the first observational evidence for high-energy

astrophysical neutrinos (Aartsen et al. 2013). The gravitational and weak forces along with the electromagnetic were added to the astronomical observations, beginning a new era of extra-galactic multi-messenger astronomy.

In 2017, LIGO detected an event consistent with a comparably nearby binary neutron-star (BNS) merger (Abbott et al. 2017a). Within seconds of the GW, the electromagnetic counterpart was observed by the Fermi Gamma Ray Burst Monitor (Abbott et al. 2017b), making this the first GW multi-messenger event. The online neutrino telescopes—including IceCube, ANTARES, and the Pierre Auger Observatory—did not detect any directionally coincident high-energy (GeV–EeV) neutrinos or an MeV neutrino burst signal (Albert et al. 2017a). While no coincident neutrinos were found, this is consistent with model predictions for the merger (Kimura et al. 2017). In contrast with BBH mergers, BNS mergers are expected to emit neutrinos at both GeV and MeV energies (Mészáros 2017).

²¹ Present address: Imperial College London, Department of Physics, Blackett Laboratory, London SW7 2AZ, UK.

²² Present address: National Institutes for Quantum and Radiological Science and Technology (QST), Hyogo 679-5148, Japan.

²³ Present address: National Research Nuclear University “MEPhI” (Moscow Engineering Physics Institute), Moscow, 115409, Russia.

²⁴ Present address: Department of Physics and Astronomy, University of Alabama, Tuscaloosa, AL 35487, USA.

²⁵ Present address: Kamioka Observatory, Institute for Cosmic-Ray Research, The University of Tokyo, Hida, Gifu 506-1205, Japan.

MeV-scale neutrinos would be produced by the hot collapsing fireball at the beginning of a gamma-ray burst (Sahu & D’Olivo 2005), so we can be confident that they must be produced when there is collapsing matter outside of a black hole. These neutrinos are modeled in several ways, but have energies on the order of the dominant photon energy, and are considerably more numerous than the emitted photons (Halzen & Jaczko 1996). In the case of a post-merger neutron star remnant, thermal emission of MeV neutrinos is expected as the remnant cools (Foucart et al. 2016). The neutron rich environment also suggests a brighter $\bar{\nu}_e$ flux than the ν_e flux (Kyutoku & Kashiyama 2018).

Recently, the LIGO/Virgo collaboration published their event catalog (Abbott et al. 2019), including the full data set from their first and second observing runs, LIGO-O1 and LIGO-O2, respectively. During the third observing run, LIGO-O3, the LIGO/Virgo collaboration initiated the online GW candidate event database (GraceDB) (LIGO Scientific Collaboration 2020), providing public alerts and a centralized location for aggregating and retrieving event information. For such transient GW events, various neutrino detectors reported correlation searches: Super-Kamiokande (Abe et al. 2016, 2018), Borexino (Agostini et al. 2017), NOvA (Acero et al. 2020), Bikal-GVD Neutrino Telescope (Avrorin et al. 2018), Daya Bay (An et al. 2020), XMASS (Collaboration et al. 2020), and IceCube/ANTARES (Adrián-Martínez et al. 2016; Albert et al. 2017b; Aartsen et al. 2020). The Kamioka Liquid scintillator AntiNeutrino Detector (KamLAND) has also performed a search for electron antineutrinos coincident with gravitational waves GW150914 and GW151226, and then candidate event LVT151012 (Gando et al. 2016a).

In this paper, we present an updated coincidence search for MeV-scale electron antineutrinos in KamLAND associated with the observed GW events in LIGO-O2 (2016 November 30–2017 August 25) and LIGO-O3 (2019 April 1–March 27).

2. KamLAND Detector

KamLAND is a large volume liquid scintillator neutrino detector located at the Kamioka mine, 1 km underground from the top of Mt. Ikenoyama in Gifu Prefecture, Japan. The KamLAND detector consists of a cylindrical 10 m radius \times 20 m height water-Cerenkov outer detector for cosmic-ray muon veto, a 9 m radius stainless steel spherical tank that mounts 1325 17 inch and 554 20 inch photomultiplier-tubes (PMTs), and a 6.5 m radius Nylon/EVOH outer balloon filled with approximately 1 kton of ultra-pure liquid scintillator. The liquid scintillator is composed of 20% Pseudocumene (1,2,4-Trimethylbenzene, C_9H_{12}), 80% Dodecane (N -12, $C_{12}H_{26}$), and 1.36 g l^{-1} PPO (2,5-Diphenyloxazole, $C_{15}H_{11}NO$). Further details of the KamLAND detector are summarized in Suzuki (2014).

KamLAND began its data acquisition in 2002 March. The detector was upgraded in 2011 August to include a drop-shaped 1.5 m radius nylon inner balloon filled with approximately 400 kg of purified xenon loaded in a liquid scintillator (Gando et al. 2016b). In this configuration, known as the KamLAND-Zen 400 experiment, KamLAND searched for neutrinoless double-beta decay until 2015 December, at which point the inner balloon was removed. Subsequently in 2018 May, a further upgrade to the KamLAND-Zen 800 experiment ensued with the addition of a 1.9 m radius inner balloon, containing approximately 800 kg of purified xenon.

Electronic boards record the digitized PMT waveforms and provide the corresponding time stamp based on a 40 MHz internal clock. All internal clocks are synchronized to the Unix Time Stamp on every 32nd pulse per second (1 PPS) trigger from a Global Positioning System receiver, located at the entrance to the Kamioka mine. Uncertainties in the absolute trigger time stamp accuracy are less than $\mathcal{O}(100)\ \mu\text{s}$, derived from the signal transportation into the mine, optical/electrical signal conversion, and triggering electronics, which is negligibly small for this coincidence search.

The interaction vertex and energy deposition are reconstructed using the measured PMT charge and timing information. At low energies, the detector calibrations are performed using various radioactive sources: ^{60}Co , ^{68}Ge , ^{203}Hg , ^{65}Zn , ^{241}Am , ^{9}Be , ^{137}Cs , and ^{210}Po , ^{13}C . At higher energies ($>10\text{ MeV}$), the energy response is calibrated using spallation-produced ^{12}B / ^{12}N . Daily stability measurements are performed using the 2.2 MeV gamma-ray emitted from a spallation-neutron capture on a proton (Abe et al. 2010). The reconstructed energy and interaction vertex resolution are evaluated as $6.4\%/\sqrt{E\ (\text{MeV})}$ and $\sim 12\ \text{cm}/\sqrt{E\ (\text{MeV})}$ (Gando et al. 2013), respectively. The primary radioactive backgrounds found in the liquid scintillator are $(5.0 \pm 0.2) \times 10^{-18}\ \text{g g}^{-1}$ ($93 \pm 4\ \text{nBq m}^{-3}$) of ^{238}U and $(1.8 \pm 0.1) \times 10^{-17}\ \text{g g}^{-1}$ ($59 \pm 4\ \text{nBq m}^{-3}$) of ^{232}Th (Gando et al. 2015).

During the period in which LIGO-O2 and LIGO-O3 were collecting data, the KamLAND detector had an average livetime efficiency of $\epsilon_{\text{live}} = 0.878$. For all but one GW event in LIGO-O2, GW170608, the KamLAND detector was actively taking physics data, whereas three GW events in LIGO-O3 (S191213g, S191215w, and S191216ap) overlapped with an unusual detector condition period. Tables 1 and 2 summarize the GW events used in this analysis during their respective observing runs, along with the KamLAND detector status.

3. Electron Antineutrino Selection and Background Estimation

In this analysis, we focus on KamLAND events induced by the electron antineutrino inverse beta-decay (IBD) reaction ($\bar{\nu}_e + p \rightarrow e^+ + n$) with 1.8 MeV neutrino energy threshold. The IBD candidate events can be selected by the delayed coincidence (DC) signature: scintillation light from the positron and its annihilation gamma-rays as a prompt signal, and a 2.2 MeV (4.9 MeV) gamma-ray from neutron capture on a proton (carbon-12) as a $207.5 \pm 2.8\ \mu\text{s}$ delayed signal (Abe et al. 2010). The incident neutrino energy (E_ν) is computed from the reconstructed prompt energy (E_{prompt}) with energy and momentum conservation in the reaction as $E_\nu \simeq E_{\text{prompt}} + 0.78\ \text{MeV} + T_n$, where T_n represents the neutron kinetic energy.

The energy range of this analysis is selected to be E_{prompt} between 0.9 and 100.0 MeV, with a delayed neutron capture on a proton (carbon-12) energy between 1.8 and 2.6 MeV (4.4–5.6 MeV). Accidental backgrounds are suppressed by imposing a spatial and time correlation between the prompt and delayed signals. In particular, the reconstructed vertex and time difference between the prompt and delayed signals must be within 200 cm and $0.5\text{--}1000\ \mu\text{s}$ of each other. All events must be reconstructed in the fiducial volume region 6 m radius from the center, corresponding to a total number of target protons of $N_T = (5.98 \pm 0.13) \times 10^{31}$. Muon and spallation vetoes are applied after the interaction of a cosmic-ray muon, which occur at a rate of approximately 0.34 Hz in KamLAND. Further

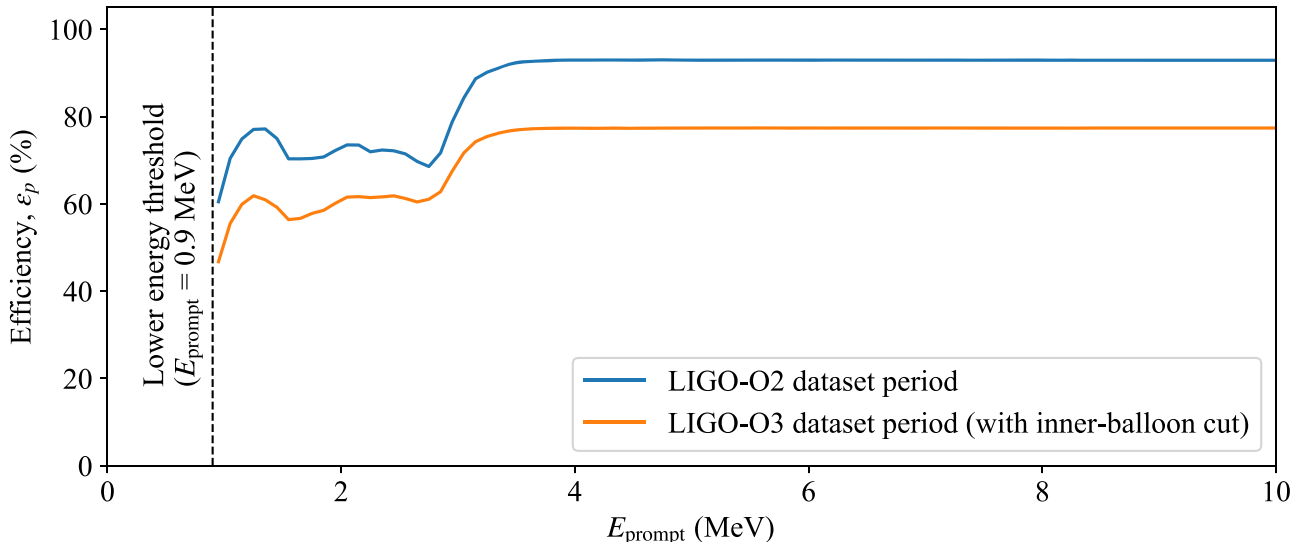


Figure 1. The electron antineutrino selection efficiencies as a function of the prompt energy. The analysis period is divided into two data sets: the LIGO-O2 period in which we use of the full fiducial volume of the KamLAND detector (blue) and the LIGO-O3 period which includes the additional inner balloon cut described in the text. At a few MeV, the selection efficiencies are reduced by the likelihood selection to suppress the contamination of accidental coincidence. The vertical dashed line represents a lower energy threshold of $E_{\text{prompt}} \geq 0.9$ MeV.

Table 1
The Gravitational Wave Event List for LIGO-O2 (Abbott et al. 2019) and along with the KamLAND Detector Status

Gravitational Wave	Date and Time (UTC)	Distance (Mpc)	Source	KamLAND Status
GW170104	2017 Jan 4, 10:11:58.6	990^{+440}_{-430}	BBH	running
GW170608	2017 Jun 8, 02:01:16.5	320^{+120}_{-110}	BBH	unusual data condition
GW170729	2017 Jul 29, 18:56:29.3	2840^{+1400}_{-1360}	BBH	running
GW170809	2017 Aug 9, 08:28:21.8	1030^{+320}_{-390}	BBH	running
GW170814	2017 Aug 14, 10:30:43.5	600^{+150}_{-220}	BBH	running
GW170817	2017 Aug 17, 12:41:04.4	40^{+7}_{-15}	BNS	running
GW170818	2017 Aug 18, 02:24:09.1	1060^{+420}_{-380}	BBH	running
GW170823	2017 Aug 23, 13:13:58.5	1940^{+970}_{-900}	BBH	running

Note. The three events in which KamLAND has already published the results for a coincidence search (Gando et al. 2016a) are not included in this table.

details regarding the event selection can be found in previous KamLAND analyses (Gando et al. 2011, 2013, 2016a; Asakura et al. 2015). A likelihood-based signal selection distinguishes electron antineutrino DC pairs from accidental coincidence backgrounds for a few to several MeV energy range. This has been updated from the previous analyses considering the accidental coincidence event rates, upgraded detector conditions of the outer detector refurbishment (Ozaki & Shirai 2017), inner balloon installation for KamLAND-Zen 800 (Gando 2020), and the activity of Japanese nuclear reactors.

From 2018 May onwards (the KamLAND-Zen 800 phase)—in order to avoid unexpected background contamination due to the xenon-loaded liquid scintillator, inner balloon body, and suspending ropes—the inner balloon region is vetoed for the delayed event. The inner-balloon cut regions are: a 2.5 m radius spherical volume centered in the detector and a 2.5 m radius vertical cylindrical volume in the upper-half of the detector. In this analysis, the effect of this additional inner balloon cut is considered as a selection efficiency suppression for the delayed event rather than a change in the number of target protons for the prompt event. Therefore, the total selection efficiencies are different between the KamLAND data sets corresponding to the periods operating during LIGO-O2 (without the inner balloon cut) and LIGO-O3 (with the additional inner balloon cut).

The selection efficiencies are shown in Figure 1, as a function of the reconstructed prompt energy ($\epsilon_p(E_{\text{prompt}})$). The structure of the efficiency suppression around $E_{\text{prompt}} \simeq 2$ MeV is primarily derived from the accidental background spectrum shape. Above $E_{\text{prompt}} = 5.0$ MeV, at which point the accidental background contamination becomes negligibly small, the selection efficiencies in each data set converge to 92.9% and 77.4%.

The dominant neutrino sources below 8 MeV are the Japanese reactor power plants and geo-chemical radioactive decays in the Earth. After the Great East Japan Earthquake on 2011 March 11, most of the reactors in Japan were shut down and only a few have since been brought back online. Other backgrounds are DC pairs of accidental radioisotopes, spallation products ^9Li , and ^{13}C (α, n) ^{16}O reaction. Above ~ 10 MeV, fast neutrons from cosmic-ray muons and atmospheric neutrino interactions are the dominant contribution to the background (Gando et al. 2012).

4. Coincidence Event Search

This analysis is performed using a coincident time window of ± 500 s around each of the 60 GW events listed in Tables 1 and 2. The selected timing window is based on the largest expected time gap between GW events and neutrino

Table 2
The Gravitational Wave Event List for LIGO-O3 (Abbott et al. 2019) and KamLAND Detector Status

Gravitational Wave	Date and Time (UTC)	KamLAND Status
S190408an	2019 Apr 8, 18:18:02	running
S190412m	2019 Apr 12, 05:30:44	running
S190421ar	2019 Apr 21, 21:38:56	running
S190425z	2019 Apr 25, 08:18:05	running
S190426c	2019 Apr 26, 15:21:55	running
S190503bf	2019 May 3, 18:54:04	running
S190510g	2019 May 10, 02:59:39	running
S190512at	2019 May 12, 18:07:14	running
S190513bm	2019 May 13, 20:54:28	running
S190517h	2019 May 17, 05:51:01	running
S190519bj	2019 May 19, 15:35:44	running
S190521g	2019 May 21, 03:02:29	running
S190521r	2019 May 21, 07:43:59	running
S190602aq	2019 Jun 2, 17:59:27	running
S190630ag	2019 Jun 30, 18:52:05	running
S190701ah	2019 Jul 1, 20:33:06	running
S190706ai	2019 Jul 6, 22:26:41	running
S190707q	2019 Jul 7, 09:33:26	running
S190718y	2019 Jul 18, 14:35:12	running
S190720a	2019 Jul 20, 00:08:36	running
S190727h	2019 Jul 27, 06:03:33	running
S190728q	2019 Jul 28, 06:45:10	running
S190814bv	2019 Aug 14, 21:10:39	running
S190828j	2019 Aug 28, 06:34:05	running
S190828i	2019 Aug 28, 06:55:09	running
S190901ap	2019 Sep 1, 23:31:01	running
S190910d	2019 Sep 10, 01:26:19	running
S190910h	2019 Sep 10, 08:29:58	running
S190915ak	2019 Sep 15, 23:57:02	running
S190923y	2019 Sep 23, 12:55:59	running
S190924h	2019 Sep 24, 02:18:46	running
S190930s	2019 Sep 30, 13:35:41	running
S190930t	2019 Sep 30, 14:34:07	running
S191105e	2019 Nov 5, 14:35:21	running
S191109d	2019 Nov 9, 01:07:17	running
S191129u	2019 Nov 29, 13:40:29	running
S191204r	2019 Dec 4, 17:15:26	running
S191205ah	2019 Dec 5, 21:52:08	running
S191213g	2019 Dec 13, 15:59:05	unusual data condition
S191215w	2019 Dec 15, 22:30:52	unusual data condition
S191216ap	2019 Dec 16, 21:33:38	unusual data condition
S191222n	2019 Dec 22, 03:35:37	running
S200105ae	2020 Jan 5, 16:24:26	running
S200112r	2020 Jan 12, 15:58:38	running
S200114f	2020 Jan 14, 02:08:18	running
S200115j	2020 Jan 15, 04:23:09	running
S200128d	2020 Jan 28, 02:20:11	running
S200129m	2020 Jan 29, 06:54:58	running
S200208q	2020 Feb 8, 13:01:17	running
S200213t	2020 Feb 13, 04:10:40	running
S200219ac	2020 Feb 19, 09:44:15	running
S200224ca	2020 Feb 24, 22:22:34	running
S200225q	2020 Feb 25, 06:04:21	running
S200302c	2020 Mar 2, 01:58:11	running
S200311bg	2020 Mar 11, 11:58:53	running
S200316bj	2020 Mar 16, 21:57:56	running

Note. Data were extracted from GraceDB (LIGO Scientific Collaboration 2020). The retracted events are not shown here.

events (Baret et al. 2011). This is sufficiently large to cover possible early neutrino emission scenarios as well as the neutrino time-of-flight delay from GW170729, the most distant

GW source in this analysis. For example, assuming the sum of neutrino mass limits and cosmological constants from Aghanim et al. (2020), and the neutrino mass-squared splittings from Esteban et al. (2019), a neutrino with an energy of 1.8 MeV, upper mass state of 60 meV, traveling a distance of 2840 Mpc will be delayed by approximately 86 s relative to the GW.

The expected number of uncorrelated background events per ± 500 s time window are estimated using off-time windows from the GW and found to be 4.08×10^{-3} and 4.27×10^{-3} for the KamLAND periods corresponding to LIGO-O2 and LIGO-O3, respectively.

No IBD electron antineutrino events were found in the KamLAND data set within ± 500 s of each GW event. Using the uncorrelated accidental background rates and zero observed signal events, the Feldman–Cousins method (Feldman & Cousins 1998) is used to derive the 90% confidence level (C.L.) upper limit on the number of detected electron antineutrinos. This is found to be $N_{90} = 2.435$ for each GW event in the LIGO-O2 and $N_{90} = 2.435$ for each GW event in the LIGO-O3. The upper limit (F_{90}) can then be used to place constraints on the neutrino fluence, as follows:

$$F_{90} = \frac{N_{90}}{N_T \epsilon_{\text{live}} \int \epsilon_s(E_{\text{prompt}}(E'_\nu)) \sigma(E'_\nu) \lambda(E'_\nu) dE'_\nu}, \quad (1)$$

where $\sigma(E_\nu)$ is the IBD cross section (Strumia & Vissani 2003) and $\lambda(E_\nu)$ is the neutrino energy spectrum. In order to perform a model independent analysis from the neutrino emission mechanisms for various GW sources, we assume a monochromatic neutrino energy spectra. Hence, we calculate 90% C.L. fluence upper limits on the electron antineutrinos for each GW event in LIGO-O2 and LIGO-O3 with

$$F_{90}(E_\nu) = \frac{N_{90}}{N_T \epsilon_{\text{live}} \epsilon_s(E_\nu) \sigma(E_\nu)}, \quad (2)$$

as shown in Figure 2. The resulting upper limits on the electron antineutrino fluence are found to be between 10^8 and 10^{13} cm^{-2} .

We study the neutrino emission energy scales between two cases of GW sources for officially published and detail-known events during LIGO-O2: the BNS merger (BNS: GW170817), and six BBH mergers (BBHs: GW170104, GW170729, GW170809, GW170814, GW170818, GW170823). Because of the ± 500 s coincidence search timing window for each event, the total number of expected background events are 4.08×10^{-3} for the BNS event and 2.45×10^{-2} for the six BBH candidates. Using the Feldman–Cousins method again with the 90% C.L., for zero events observed, the upper limit on the number of neutrino events is $N_{90}^{\text{BNS}} = 2.435$ and $N_{90}^{\text{BBHs}} = 2.415$ for the BNS and the BBHs, respectively. According to Kyutoku & Kashiyama (2018), the assumption that the neutrino energy spectrum has a Fermi–Dirac distribution is reasonable for exploring the mechanism of neutrino emissions from the GW sources. Assuming the Fermi–Dirac distribution, the neutrino energy spectra can be written as

$$\lambda_{\text{FD}}(E_\nu) = \frac{1}{T^3 f_2(\eta)} \frac{E_\nu^2}{e^{E_\nu/T-\eta} + 1}, \quad (3)$$

$$f_n(\eta) = \int_0^\infty \frac{x^n}{e^{x-\eta} + 1} dx, \quad (4)$$

where we assume zero chemical potential and pinching factor $\eta = 0$, the temperature is given as $T = \langle E \rangle / 3.15$, and the

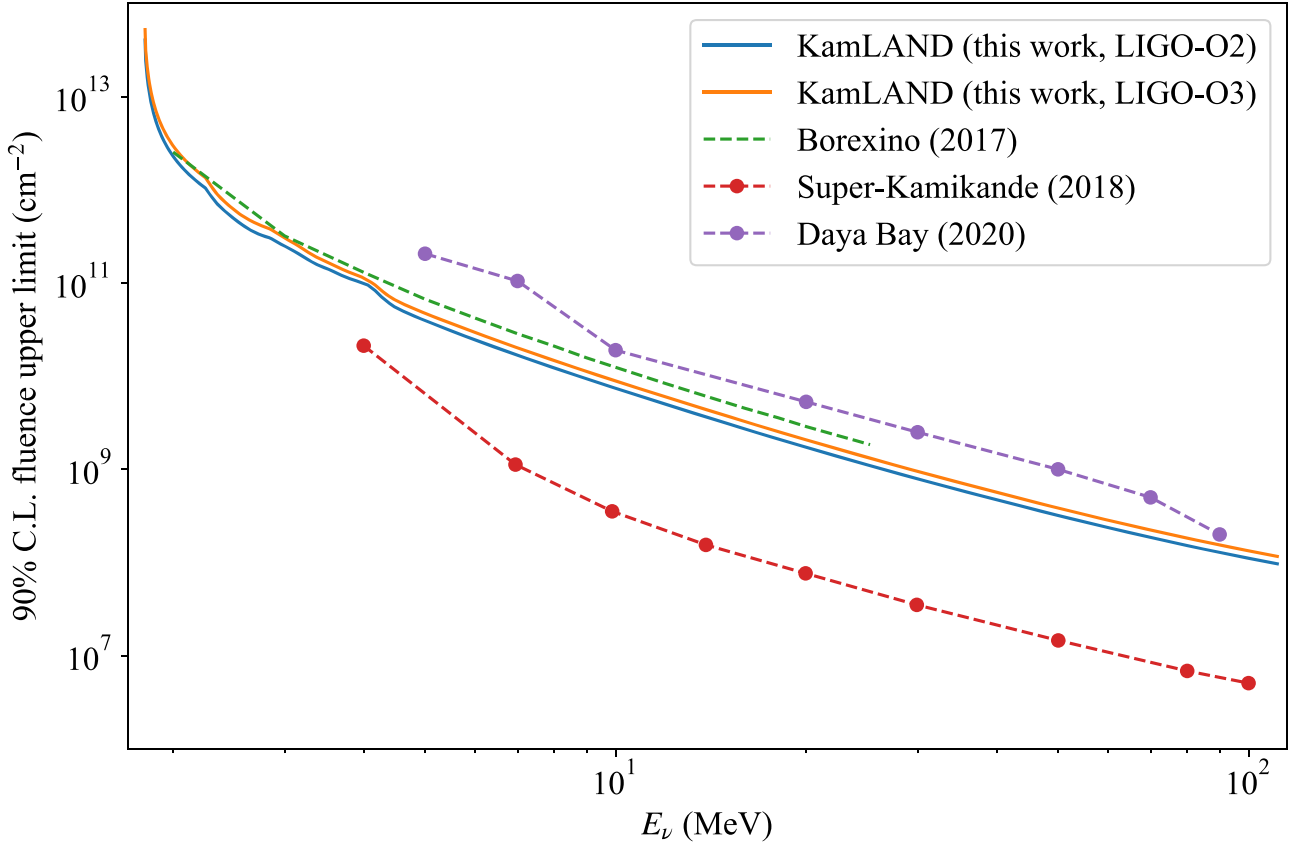


Figure 2. The 90% C.L. electron antineutrino fluence upper limits for each GW. The limits corresponding to events from LIGO-O2 are shown in blue, and events from LIGO-O3 are shown in orange. The difference between the two upper limits are primarily driven by the different selection efficiencies shown in Figure 1. For comparison, the 90% C.L. fluence upper limits on electron antineutrinos are also shown for Super-Kamiokande (Abe et al. 2018): GW170817; Borexino (Agostini et al. 2017): GW150914, GW151226, and GW170104; and Daya Bay (An et al. 2020): average of GW150914, GW151012, GW151226, GW170104, GW170608, GW170814, and GW170817. Borexino result as the un-binned analysis is shown as a green dashed line, Super-Kamiokande and Daya Bay results with binned analysis are shown as red dots and purple dots, respectively.

average neutrino energy $\langle E \rangle = 12.7$ MeV (Caballero et al. 2016). Integrating between the true electron antineutrino energy limits, $E_\nu = 1.8\text{--}111$ MeV, following Equation (1) and assuming equal contribution from six neutrino species, we obtain upper limits on the total fluence ($\mathcal{F}_{90}^{\text{BNS, BBH}}$) in the Fermi–Dirac distribution case with 90% C.L. as

$$\mathcal{F}_{90}^{\text{BNS}} \leq 2.04 \times 10^{10} \text{ cm}^{-2} \quad (5)$$

for the BNS and

$$\mathcal{F}_{90}^{\text{BBH}} \leq 2.02 \times 10^{10} \text{ cm}^{-2} \quad (6)$$

for the BBH. Considering the luminosity distances from the GW source, we convert the total fluence (\mathcal{F}_{90}) to the total energy (\mathcal{L}_{90}) radiated in neutrinos from single source as

$$\mathcal{L}_{90}^{\text{BNS, BBH}} = \frac{\mathcal{F}_{90}^{\text{BNS, BBH}}}{1/(4\pi D_{\text{eff}}^2 \langle E \rangle)}, \quad (7)$$

where D_{eff} is the effective distance defined as $1/D_{\text{eff}}^2 \equiv \sum_i 1/D_i^2$ for every i th GW event, and the central values are used to D_i . Hence, the upper limits on the total energy are obtained as

$$\mathcal{L}_{90}^{\text{BNS}} \leq 7.92 \times 10^{58} \text{ erg} \quad (8)$$

based on the 40 Mpc distance to the BNS event, and

$$\mathcal{L}_{90}^{\text{BBH}} \leq 8.22 \times 10^{60} \text{ erg} \quad (9)$$

for the BBHs based on the effective distance of 407.6 Mpc, without accounting for neutrino oscillation effects. The observed upper limits are found to be larger than the typical total energy radiated from supernovae $\mathcal{O}(10^{53})$ erg (Bethe 1990).

5. Summary

This paper searched for coincident IBD electron antineutrinos in KamLAND with the 60 GW events associated with the second and third observing runs of the LIGO detector. No coincident signal was observed within a ± 500 s timing window around each GW event. The 90% C.L. electron antineutrino fluence upper limit for each GW, assuming a mono-energetic neutrino flux, was presented for neutrino energies between 1.8 and 111 MeV. We set the most strict upper limit on each GW event in the LIGO-O2 data set below 3.5 MeV neutrino energies. For the LIGO-O3 data set, this is the first result of an MeV-scale energy coincidence neutrino search.

The obtained upper limits on the total energy radiated from GW source class, BNS or BBH, in LIGO-O2 with the assumption of a Fermi–Dirac neutrino energy distribution, are found to be 7.92×10^{58} erg and 8.22×10^{60} erg, respectively. These results depend on the number of GW events and distances. This limit will be improved once the candidate events of LIGO-O3 are published.

In the future, the mechanism of neutrino emission may be constrained and explored by combining with multi-messenger

astronomy: GeV/TeV neutrino detectors, X-ray/gamma-ray telescopes, and gravitational wave detectors. The KamLAND detector continues to take physics data while running in the KamLAND-Zen 800 configuration and is monitoring for transient astrophysical events. The recently implemented online monitor at KamLAND (Asakura et al. 2016) also readily searches for correlations with transient events and reports the results to the Gamma-ray Coordinates Network (GCN) and/or the Astronomer’s Telegram (ATel).

The KamLAND experiment is supported by JSPS KAKENHI Grants 19H05803; the World Premier International Research Center Initiative (WPI Initiative), MEXT, Japan; Netherlands Organisation for Scientific Research (NWO); and under the U.S. Department of Energy (DOE) Contract No. DE-AC02-05CH11231, the National Science Foundation (NSF) No. NSF-1806440, NSF-2012964, as well as other DOE and NSF grants to individual institutions. The Kamioka Mining and Smelting Company has provided service for activities in the mine. We acknowledge the support of NII for SINET4. This work is partly supported by the Graduate Program on Physics for the Universe (GP-PU), and the Frontier Research Institute for Interdisciplinary Sciences, Tohoku University.

ORCID iDs

K. Ishidoshiro  <https://orcid.org/0000-0001-9271-2301>
 N. Kawada  <https://orcid.org/0000-0003-2350-2786>
 H. Watanabe  <https://orcid.org/0000-0002-2363-5637>
 S. Obara  <https://orcid.org/0000-0003-3488-3553>
 B. K. Fujikawa  <https://orcid.org/0000-0002-7001-717X>
 A. Li  <https://orcid.org/0000-0002-4844-9339>
 M. P. Decowski  <https://orcid.org/0000-0002-1577-6229>

References

Aartsen, M., Abbasi, R., Abdou, Y., et al. 2013, *Sci*, 342, 1242856
 Aartsen, M. G., Ackermann, M., Adams, J., et al. 2020, *ApJL*, 898, L10
 Abbott, B. P., Abbott, R., Abbott, T., et al. 2017a, *PhRvL*, 119, 161101
 Abbott, B. P., Abbott, R., Abbott, T. D., et al. 2016, *PhRvL*, 116, 061102
 Abbott, B. P., Abbott, R., Abbott, T. D., et al. 2017b, *ApJL*, 848, L12
 Abbott, B. P., Abbott, R., Abbott, T. D., et al. 2019, *PhRvX*, 9, 031040
 Abe, K., Bronner, C., Hayato, Y., et al. 2018, *ApJL*, 857, L4
 Abe, K., Haga, K., Hayato, Y., et al. 2016, *ApJL*, 830, L11
 Abe, S., Enomoto, S., Furuno, K., et al. 2010, *PhRvC*, 81, 025807
 Acero, M. A., Adamson, P., Aliaga, L., et al. 2020, *PhRvD*, 101, 112006
 Adrián-Martínez, S., Albert, A., André, M., et al. 2016, *PhRvD*, 93, 122010
 Aghanim, N., Akrami, Y., Ashdown, M., et al. 2020, *A&A*, 641, A6
 Agostini, M., Altenmüller, K., Appel, S., et al. 2017, *ApJ*, 850, 21
 Albert, A., André, M., Anghinolfi, M., et al. 2017a, *ApJL*, 850, L35
 Albert, A., André, M., Anghinolfi, M., et al. 2017b, *PhRvD*, 96, 022005
 An, F. P., Balantekin, A. B., Band, H. R., et al. 2020, arXiv:2006.15386
 Asakura, K., Gando, A., Gando, Y., et al. 2015, *ApJ*, 806, 87
 Asakura, K., Gando, A., Gando, Y., et al. 2016, *ApJ*, 818, 91
 Avrorin, A. D., Avrorin, A. V., Aynutdinov, V. M., et al. 2018, *JETPL*, 108, 787
 Baret, B., Bartos, I., Bouhou, B., et al. 2011, *APh*, 35, 1
 Bethe, H. A. 1990, *RvMP*, 62, 801
 Caballero, O. L., Zielinski, T., McLaughlin, G. C., & Surman, R. 2016, *PhRvD*, 93, 123015
 Collaboration, X., Abe, K., Hiraide, K., et al. 2020, arXiv:2007.16046
 Esteban, I., Gonzalez-Garcia, M., Hernandez-Cabezudo, A., Maltoni, M., & Schwetz, T. 2019, *JHEP*, 2019, 106
 Feldman, G. J., & Cousins, R. D. 1998, *PhRvD*, 57, 3873
 Foucart, F., Haas, R., Duez, M. D., et al. 2016, *PhRvD*, 93, 044019
 Gando, A., Gando, Y., Hachiya, T., et al. 2016a, *ApJL*, 829, L34
 Gando, A., Gando, Y., Hachiya, T., et al. 2016b, *PhRvL*, 117, 082503
 Gando, A., Gando, Y., Hanakago, H., et al. 2013, *PhRvD*, 88, 033001
 Gando, A., Gando, Y., Hanakago, H., et al. 2015, *PhRvC*, 92, 055808
 Gando, A., Gando, Y., Ichimura, K., et al. 2011, *NatGe*, 4, 647
 Gando, A., Gando, Y., Ichimura, K., et al. 2012, *ApJ*, 745, 193
 Gando, Y. 2020, *JPhCS*, 1468, 012142
 Halzen, F., & Jaczko, G. 1996, *PhRvD*, 54, 2779
 Kimura, S. S., Murase, K., Mészáros, P., & Kiuchi, K. 2017, *ApJL*, 848, L4
 Kyutoku, K., & Kashiyama, K. 2018, *PhRvD*, 97, 103001
 LIGO Scientific Collaboration 2020, GraceDB, <https://gracedb.ligo.org/superevents/public/O3/>
 Mészáros, P. 2017, Gamma-Ray Bursts as Neutrino Sources (Singapore: World Scientific), 1
 Ozaki, H., & Shirai, J. 2017, in 38th International Conference on High Energy Physics (ICHEP2016) (Trieste: SISSA), 1161
 Sahu, S., & D’Olivo, J. C. 2005, *PhRvD*, 71, 047303
 Strumia, A., & Vissani, F. 2003, *PhLB*, 564, 42
 Suzuki, A. 2014, *EPJC*, 74, 3094